Statistical multifragmentation model with discretized energy and the generalized Fermi breakup: Formulation of the model

S. R. Souza,[1,2] B. V. Carlson,[3] R. Donangelo,[1,4] W. G. Lynch,[5] and M. B. Tsang[5]

[1]*Instituto de Física, Universidade Federal do Rio de Janeiro Cidade Universitária, CP 68528, 21941-972 Rio de Janeiro, Brazil*

[2]*Instituto de Física, Universidade Federal do Rio Grande do Sul, Avenida Bento Gonçalves 9500, CP 15051, 91501-970 Porto Alegre, Brazil*

[3]*Departamento de Física, Instituto Tecnológico de Aeronáutica–CTA, 12228-900 São José dos Campos, Brazil*

[4]*Instituto de Física, Facultad de Ingeniería, Universidad de la República, Julio Herrera y Reissig 565, 11.300 Montevideo, Uruguay*

[5]*National Superconducting Cyclotron Laboratory and Department of Physics and Astronomy Department, Michigan State University, East Lansing, Michigan 48824, USA*

(Received 10 May 2013; revised manuscript received 24 June 2013; published 18 July 2013)

The generalized Fermi breakup model, recently demonstrated to be formally equivalent to the statistical multifragmentation model, if the contribution of excited states is included in the state densities of the former, is implemented. Because this treatment requires application of the statistical multifragmentation model repeatedly on hot fragments until they have decayed to their ground states, it becomes extremely computationally demanding, making its application to the systems of interest extremely difficult. Based on exact recursion formulas previously developed by Chase and Mekjian to calculate statistical weights very efficiently, we present an implementation which is efficient enough to allow it to be applied to large systems at high excitation energies. Comparison with the GEMINI++ sequential decay code and the Weisskopf-Ewing evaporation model shows that the predictions obtained with our treatment are fairly similar to those obtained with these more traditional models.

DOI: 10.1103/PhysRevC.88.014607 PACS number(s): 25.70.Pq, 24.60.−k

I. INTRODUCTION

The theoretical understanding of many nuclear processes requires treatment of the de-excitation of reaction products, as most of them have already decayed (typically within 10^{-20} s) by the time they are observed at the detectors (after 10^{-9} s). Owing to the great complexity associated with the theoretical description of nuclear decay, different approaches have been developed over many decades, ranging from the pioneering fission treatment of Bohr-Wheeler [1] and the Weisskopf-Ewing statistical emission [2] to the modern GEMINI binary decay codes [3] and GEMINI++ [4,5], which generalize the Bohr-Wheeler treatment. Many other models, which focus on different aspects of the de-excitation process, such as pre-equilibrium emission, have also been developed by other groups (see Ref. [6] for an extensive review of the statistical decay treatments).

The decay of complex fragments produced in reactions that lead to relatively hot sources, whose temperature is higher than approximately 4 MeV, has often been described by simpler models, owing to the very large number of primary hot fragments produced in different reaction channels, making the need for computational efficiency at least as important as the corresponding accuracy. For this reason, treatments based on the Weisskopf-Ewing decay and the Fermi breakup model [7,8] have been extensively employed [9,10] in these cases. More evolved schemes, such as the MSU decay [11,12], which incorporates much empirical information besides employing the GEMINI code and the Hauser-Feshbach formalism [13] where such information is not available, have also been developed.

Recently, a generalization of the Fermi breakup model (GFBM), including contributions from the density of excited states, has been proposed in Ref. [14] and demonstrated to be formally equivalent to the statistical multifragmentation model (SMM) [15–17]. However, the inclusion of the density of excited states makes the GFBM considerably more computationally involved than its simplified traditional version [9], in which very few discrete excited states are considered. It therefore makes the application of the GFBM to the systems of interest a very difficult task, as a very large number of breakup channels has to be taken into account for large and highly excited systems, such as those considered in multifragment emission [10,12]. Because in the framework of the GFBM the SMM should be repeatedly applied to calculate the decay of hot fragments, application of the model to large systems and high excitation energies becomes almost prohibitively time-consuming.

In this work, we present an implementation of the GFBM based on the exact recursion formulas developed by Chase and Mekjian [18] and further developed in subsequent works [12,19–21] to calculate the partition function. Because this scheme allows the calculation of statistical weights to be performed with a high efficiency, it turns out to be well suited to speeding up the very computationally demanding calculations needed in the GFBM.

We thus start, in Sec. II, by reviewing the SMM, on which the model is based, and also discuss the recursion relations just mentioned. A comparison of the results obtained with the Monte Carlo version of the SMM and that based on these recursion formulas, which we call the SMM with discrete energy (SMM-DE), is also made. Then, in Sec. III we work out the implementation of the GFBM and discuss some results. Concluding remarks are made in Sec. IV.

II. PRIMARY FRAGMENTS

In the framework of the SMM [15–17], an excited source, with A_0 nucleons, Z_0 protons, and excitation energy E^*,

undergoes a prompt breakup. Hot primary fragments are thus produced, except for those which have no internal degrees of freedom and are therefore cold, i.e., nuclei whose mass number $A \leqslant 4$, except for α particles. Partitions consistent with mass, charge, and energy conservation are generated and the corresponding statistical weights are calculated. In Sec. II A, we briefly review the main features of the SMM. The implementation based on the discretization of the energy, using the recurrence relations developed by Pratt and Das Gupta [21], is discussed in Sec. II B. A comparison between the two implementations is made in Sec. II C.

A. The SMM model

In each fragmentation mode f, the multiplicity $n_{A,Z}$ of a species, possessing mass and atomic numbers A and Z, respectively, must fulfill the constraints:

$$A_0 = \sum_{\{A,Z\}} A\, n_{A,Z} \quad \text{and} \quad Z_0 = \sum_{\{A,Z\}} Z\, n_{A,Z}. \tag{1}$$

The statistical weight Ω_f associated with the fragmentation mode $f = \{n_{A,Z}\}$ is given by the number of microstates associated with it:

$$\Omega_f(E) = \exp(S_f), \tag{2}$$

where $E = -B_{A_0,Z_0} + E^*$ denotes the total energy of the system, B_{A_0,Z_0} represents the binding energy of the source, and S_f corresponds to the total entropy of the fragmentation mode:

$$S_f = \sum_{\{A,Z\}} n_{A,Z} S_{A,Z}. \tag{3}$$

The entropy $S_{A,Z}$ is obtained through the standard thermodynamical relation:

$$S = -\frac{dF}{dT}. \tag{4}$$

In the above expression, T denotes the breakup temperature and $F_{A,Z}$ is the Helmholtz free energy associated with the species, which is related to its energy $E_{A,Z}$ through

$$E = F + TS. \tag{5}$$

The breakup temperature of the fragmentation mode f is obtained through the energy conservation constraint:

$$E^* - B_{A_0,Z_0} = C_c \frac{Z_0^2}{A_0^{1/3}} \frac{1}{(1+\chi)^{1/3}} + \sum_{\{A,Z\}} n_{A,Z} E_{A,Z}(T_f), \tag{6}$$

where the subindex f was used in T_f to emphasize the fact that the breakup temperature varies from one partition to another [22], although we drop this subindex from now on to simplify the notation. In the above equation, the first term on the right-hand side corresponds to the Coulomb energy of a uniform sphere of volume $V = (1+\chi)V_0$, $\chi > 0$, where V_0 denotes the ground-state volume of the source and C_c is a parameter (see below). In this work, we use $\chi = 2$ in all calculations. The fragment energy $E_{A,Z}(T)$ reads

$$E_{A,Z}(T) = -B_{A,Z} + \epsilon^*_{A,Z} - C_c \frac{Z^2}{A^{1/3}} \frac{1}{(1+\chi)^{1/3}} + E^{\text{trans}}_{A,Z}, \tag{7}$$

where $B_{A,Z}$ stands for the fragment's binding energy, $\epsilon^*_{A,Z}$ denotes the internal excitation energy of the fragment, and the contribution $E^{\text{trans}}_{A,Z}$ to the total kinetic energy E^{trans} reads

$$E^{\text{trans}} = \sum_{\{A,Z\}} n_{A,Z} E^{\text{trans}}_{A,Z} = \frac{3}{2}(M-1)T, \tag{8}$$

where $M = \sum_{\{A,Z\}} n_{A,Z}$ is the total multiplicity of the fragmentation mode f. The factor $M-1$, rather than M, takes into account the fact that the center of mass is at rest. Together with the Coulomb terms in the fragments' binding energies and that of the homogeneous sphere in Eq. (6), the Coulomb contribution on the right-hand side of Eq. (7) adds up to account for the Coulomb energy of the fragmented system in the Wigner-Seitz approximation [15,23].

In Ref. [11], empirical values were used for $B_{A,Z}$ and an extrapolation scheme was developed to the mass region where experimental information is not available. For simplicity, in this work, except for $A \leqslant 4$, in which case empirical values are used, we adopt the mass formula developed in Ref. [24]:

$$B_{A,Z} = C_v A - C_s A^{2/3} - C_c \frac{Z^2}{A^{1/3}} + C_d \frac{Z^2}{A} + \delta_{A,Z} A^{-1/2}, \tag{9}$$

where

$$C_i = a_i \left[1 - k\left(\frac{A-2Z}{A}\right)^2\right] \tag{10}$$

and $i = v, s$ denotes the volume and surface terms, respectively. The last term in Eq. (9) is the usual pairing contribution:

$$\delta_{A,Z} = \tfrac{1}{2}[(-1)^{A-Z} + (-1)^Z] C_p. \tag{11}$$

We refer the reader to Ref. [24] for numerical values of the parameters.

In the standard version of the SMM [15], the contribution to the entropy and the fragment's energy owing to the internal degrees of freedom is obtained from the internal Helmholtz free energy:

$$F^*_{A,Z}(T) = -\frac{T^2}{\epsilon_0} A + \beta_0 A^{2/3} \left[\left(\frac{T_c^2 - T^2}{T_c^2 + T^2}\right)^{5/4} - 1\right], \tag{12}$$

where $T_c = 18.0$ MeV, $\beta_0 = 18.0$ MeV, and $\epsilon_0 = 16.0$ MeV. In Ref. [11], effects associated with discrete excited states have been incorporated into $F^*_{A,Z}(T)$. For simplicity, in the present work, we only use the above expression.

Finally, the total contribution to the entropy associated with the translational motion reads

$$F_{\text{trans}} = -T(M-1)\log\left(V_f/\lambda_T^3\right) + T\log\left(A_0^{3/2}\right) - T\sum_{\{A,Z\}} n_{A,Z}\left[\log(g_{A,Z} A^{3/2}) - \frac{1}{n_{A,Z}}\log(n_{A,Z}!)\right]. \tag{13}$$

In the above expression, $V_f = \chi V_0$ denotes the free volume, and the factor $M-1$, as well as the term $T\log(A_0^{3/2})$, arises from the constraint that the center of mass be at rest [14,25]. The thermal wavelength reads $\lambda_T = \sqrt{2\pi\hbar^2/m_n T}$, where m_n

is the nucleon mass. Empirical values of the spin degeneracy factors $g_{A,Z}$ are used for $A \leqslant 4$. In the case of heavier nuclei, we set $g_{A,Z} = 1$ as (to some extent) this is taken into account by $F^*_{A,Z}$.

Fragmentation modes are generated by carrying out the following steps.

(i) The multiplicities $\{n_{A,Z}\}$ are sampled under the constraints imposed by Eq. (1), as described in Ref. [17].
(ii) Equation (6) is solved in order to determine the breakup temperature T.
(iii) The total entropy is calculated through Eqs. (3) and (4), after having computed the Helmholtz free energies from Eqs. (12) and (13).

The average value of an observable O is then calculated through

$$\overline{O} = \frac{\sum_f \Omega_f(E) O_f}{\sum_f \Omega_f(E)}. \tag{14}$$

Because hundreds of millions of partitions must be generated in order to achieve a reasonable sampling of the available phase space, this implementation, although feasible, is time-consuming. It has been quite successful in describing several features of the multifragmentation process [10].

B. The SMM-DE model

A much more efficient scheme has been proposed by Chase and Mekjian [18], who developed an exact method based on recursion formulas. This allows one to easily compute the number of states Ω_A associated with the breakup of a nucleus of mass number A in the canonical ensemble through [19]

$$\Omega_A = \sum_{\{\sum_k n_k a_k = A\}} \prod_k \frac{\omega_k^{n_k}}{n_k!} = \sum_{a=1}^{A} \frac{a}{A} \omega_a \Omega_{A-a}, \tag{15}$$

where ω_k denotes the number of states of a nucleus of mass number a.

This result was later generalized to distinguish protons from neutrons, leading to a similar expression [20]:

$$\begin{aligned}\Omega_{A,Z} &= \sum_{\{\sum_\alpha n_{a_\alpha,z_\alpha} \zeta_\alpha = \Lambda\}} \prod_\alpha \frac{(\omega_{a_\alpha,z_\alpha})^{n_{a_\alpha,z_\alpha}}}{n_{a_\alpha,z_\alpha}!} \\ &= \sum_\alpha \frac{\zeta_\alpha}{\Lambda} \omega_{a_\alpha,z_\alpha} \Omega_{A-a_\alpha,Z-z_\alpha},\end{aligned} \tag{16}$$

where Λ denotes A or Z, and ζ_α conveniently represents either a_α or z_α. Although somewhat more involved than the previous expression, it still allows one to calculate the statistical weight associated with the breakup of a nucleus (A, Z) very efficiently, as well as other average quantities, such as the average multiplicities [20]:

$$\begin{aligned}\overline{n}_{a,z} &= \frac{1}{\Omega_{A,Z}} \sum_{\{\sum_\alpha n_{a_\alpha,z_\alpha} \zeta_\alpha = \Lambda\}} n_{a,z} \prod_\alpha \frac{(\omega_{a_\alpha,z_\alpha})^{n_{a_\alpha,z_\alpha}}}{n_{a_\alpha,z_\alpha}!} \\ &= \frac{\omega_{a,z}}{\Omega_{A,Z}} \Omega_{A-a,Z-z}.\end{aligned} \tag{17}$$

This scheme has been successfully applied to the description of the breakup of excited nuclear systems during the last decade [12].

The extension to the microcanonical ensemble was developed in Ref. [21]. More specifically, Eq. (6) can be rewritten as

$$Q\Delta_Q \equiv E^* - B^c_{A_0,Z_0} = \sum_{\alpha,q_\alpha} q_\alpha \Delta_Q n_{\alpha,q_\alpha}, \tag{18}$$

where $q_\alpha \Delta_Q$ denotes the fragment's energy, together with the corresponding Wigner-Seitz contribution to the Coulomb energy:

$$q_{A,Z}\Delta_Q = -B^c_{A,Z} + \epsilon^*_{A,Z} + E^{\text{trans}}_{A,Z} \tag{19}$$

and

$$B^c_{A,Z} \equiv B_{A,Z} + C_c \frac{Z^2}{A^{1/3}} \frac{1}{(1+\chi)^{1/3}}. \tag{20}$$

In contrast to the continuous quantities E and $E_{A,Z}$, Q and $q_{A,Z}$ are discrete. The granularity of the discretization is conveniently regulated by the energy bin Δ_Q. In this way, Q may be treated as a conserved quantity, similarly to the mass and atomic numbers, so that the recursion relation now reads [21]

$$\Omega_{A,Z,Q} = \sum_{\alpha,q_\alpha} \frac{a_\alpha}{A} \omega_{a_\alpha,z_\alpha,q_\alpha} \Omega_{A-a_\alpha,Z-z_\alpha,Q-q_\alpha}, \tag{21}$$

and the average multiplicity is given by

$$\overline{n}_{a,z,q} = \frac{\omega_{a,z,q}}{\Omega_{A_0,Z_0,Q}} \Omega_{A_0-a,Z_0-z,Q-q}. \tag{22}$$

Other average quantities, such as the breakup temperature and the total entropy, can also be readily obtained:

$$\frac{1}{T} = \frac{\partial \ln\left(\Omega_{A_0,Z_0,Q}\right)}{\partial(Q\Delta_Q)} \approx \frac{\ln\left(\Omega_{A_0,Z_0,Q}\right) - \ln\left(\Omega_{A_0,Z_0,Q-1}\right)}{\Delta_Q} \tag{23}$$

and

$$S = \ln\left(\Omega_{A_0,Z_0,Q}\right). \tag{24}$$

The statistical weight $\{\Omega_{A,Z,q}\}$ is determined once $\omega_{A,Z,q}$ has been specified. The latter is obtained by folding the number of states associated with the kinetic motion with that corresponding to the internal degrees of freedom,

$$\omega_{A,Z,q} = \gamma_A \int_0^{\epsilon_{A,Z,q}} dK\ \sqrt{K}\, \rho^*_{A,Z}(\epsilon_{A,Z,q} - K), \tag{25}$$

where

$$\gamma_A = \Delta_Q \frac{V_f (2m_n A)^{3/2}}{4\pi^2 \hbar^3}, \tag{26}$$

$\epsilon_{A,Z,q} \equiv q\Delta_Q + B^c_{A,Z}$, and $\rho^*_{A,Z}(\epsilon^*)$ is the density of the internal states of the nucleus (A, Z) with excitation energy ϵ^*. It thus becomes clear that the fundamental physical ingredient is $\rho^*_{A,Z}(\epsilon^*)$, as it plays a major role in the determination of the statistical weight.

Because $\Omega_{A,Z,q}$ depends on three variables and the calculation of $\omega_{A,Z,q}$ usually must be evaluated numerically, the computation of $\Omega_{A_0,Z_0,Q}$ may be very time-consuming for big sources, large excitation energies, and small values of

Δ_Q (large Q). Nevertheless, $\omega_{A,Z,q}$ and $\Omega_{A,Z,q}$ need to be calculated only once and may be stored in order to considerably speed up future calculations, even for different sources, as these quantities do not depend on the source's properties. This is the strategy we adopt.

In Ref. [11], it was shown that the standard SMM internal free energy is fairly well approximated over a wide range of temperatures if one adopts the following density of states:

$$\rho^*_{A,Z}(\epsilon^*) = \rho_{\rm SMM}(\epsilon^*) = \rho_{\rm FG}(\epsilon^*) e^{-b_{\rm SMM}(a_{\rm SMM}\epsilon^*)^{3/2}}, \quad (27)$$

with

$$\rho_{\rm FG}(\epsilon^*) = \frac{a_{\rm SMM}^{1/4}}{\sqrt{4\pi}\epsilon^{*3/4}} \exp(2\sqrt{a_{\rm SMM}\epsilon^*}) \quad (28)$$

and

$$a_{\rm SMM} = \frac{A}{\epsilon_0} + \frac{5}{2}\beta_0 \frac{A^{2/3}}{T_c^2}. \quad (29)$$

The parameter $b_{\rm SMM} = 0.07A^{-\tau}$, $\tau = 1.82(1 + A/4500)$, for $A > 4$. In the case of the α particles, we set $\beta_0 = 0$ and $b_{\rm SMM} = 0.000848416$. For the other light nuclei whose $A < 5$, which have no internal degrees of freedom, we use $\rho^*_{A,Z}(\epsilon^*) = g_{A,Z}\delta(\epsilon^*)$.

As mentioned above, we call this implementation of the model SMM-DE.

C. Comparison with the SMM

In order to investigate the extent to which the above implementations of the SMM agree with each other, we show in Fig. 1 the caloric curve predicted by both versions of the SMM for the breakup of the ^{40}Ca nucleus. As expected, at low temperatures, the caloric curve is very close to that of a Fermi gas but this behavior quickly changes for $E^*/A \gtrsim 2$ MeV, as the fragment multiplicity M starts to deviate from 1 (see top panel in Fig. 4). From this point on, the temperature rises more slowly than that of a Fermi gas as the excitation energy increases, owing to the higher heat capacity of the system, which progressively produces more fragments with internal degrees of freedom, besides very light ones.

Comparison between the results obtained with the SMM and those with the SMM-DE shows that both versions predict very similar caloric curves. To some extent, slight deviations should be expected, as there are small differences between the two implementations. First, in the SMM the constraint on the center-of-mass motion is taken into account by Eqs. (8) and (13), whereas it is ignored in the SMM-DE. Therefore, the latter has more states than the former, leading to different statistical weights and, as a consequence, different averages. Second, as pointed out in Ref. [21], for a given fragmentation mode, fluctuations around the mean excitation energy of each fragment are not allowed in the SMM, whereas the summation over q in Eq. (21) considers all possible ways of sharing the energy among the fragments. The results nonetheless reveal that the practical consequences of these two points are small.

The comparison of the results obtained with $\Delta_Q = 0.2$ MeV versus $\Delta_Q = 1.0$ MeV, also displayed in Fig. 1, shows that this parameter should have little influence on the results. This is of particular relevance, as the numerical effort increases very rapidly as Δ_Q decreases, which makes the application of the model for big systems at high excitation energies much more time-consuming. We use $\Delta_Q = 0.2$ MeV in the remainder of this work, but these results suggest that somewhat larger values would be just as good.

More detailed information on the similarities of the two versions of the SMM may be obtained by examining the charge distribution of the primary fragments produced at different excitation energies, as shown in Fig. 2. One also sees in this case that both SMM calculations lead to very similar predictions, although small deviations are observed. They are more pronounced in the Z region close to the source size, as its contribution is overestimated in the SMM-DE. However, the differences in lower Z regions are smaller and should

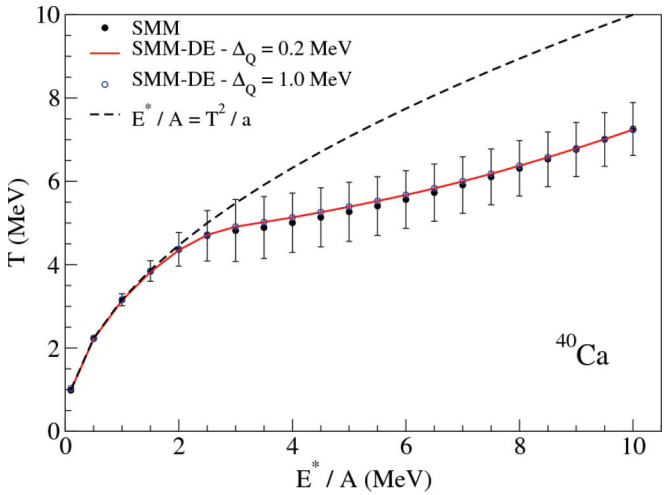

FIG. 1. (Color online) Caloric curve predicted by the SMM and the SMM-DE for the ^{40}Ca. The dashed line represents a Fermi gas with $a = 10$ MeV. For details see the text.

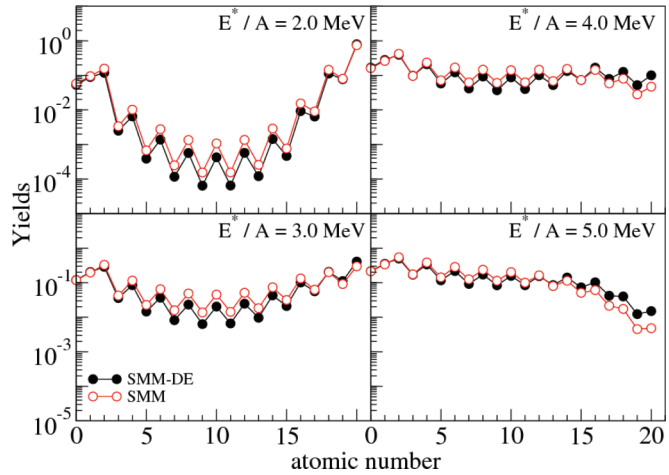

FIG. 2. (Color online) Charge distribution of the hot primary fragments from the breakup of ^{40}Ca, obtained with the different versions of the SMM at selected excitation energies. For details see the text.

not impact the conclusions drawn from either implementation, within the usual uncertainties of these calculations. We therefore believe that either implementation of the SMM can be safely adopted.

III. DE-EXCITATION OF PRIMARY FRAGMENTS

In Ref. [14], it has been demonstrated that the statistical description of the multifragment emission made by the SMM is equivalent to a generalized version of the Fermi breakup, in which the excited states of the fragments are included. We here pursue this idea and apply it to the description of de-excitation of the hot primary fragments, referring the reader to that work for a detailed discussion.

The starting point is Eq. (22), which provides the average multiplicity $\overline{n}_{a,z,q}$ of a fragment (a, z) with total energy $q\Delta_Q$, produced in the breakup of a source (A_0, Z_0) with total energy $Q\Delta_Q$. The average excitation energy $\overline{\epsilon}^*$ of the fragment is calculated through

$$\overline{\epsilon}^* = \frac{\gamma_a}{\omega_{a,z,q}} \int_0^{\epsilon_{a,z,q}} dK\ (\epsilon_{a,z,q} - K)\sqrt{K}\rho^*_{a,z}(\epsilon_{a,z,q} - K). \tag{30}$$

In Fig. 3 we denote by $n(\overline{\epsilon}^*)$ the average multiplicity of C isotopes with energy $q\Delta_Q$, i.e., $\overline{n}_{A,6,q}$, and plot this quantity, scaled by the corresponding maximum value, as a function of the average excitation energy $\overline{\epsilon}^*$. The results were obtained from the breakup of ^{40}Ca at $E^*/A = 3$, 5, and 7 MeV. One notes that $\overline{\epsilon}^*$ is very broad and that the width of the distribution becomes larger as E^*/A increases. The average value of $\overline{\epsilon}^*$ also shifts to higher values as the excitation energy of the source E^*/A becomes higher. It is clear from these results that the internal excitation of the fragments cannot be neglected and

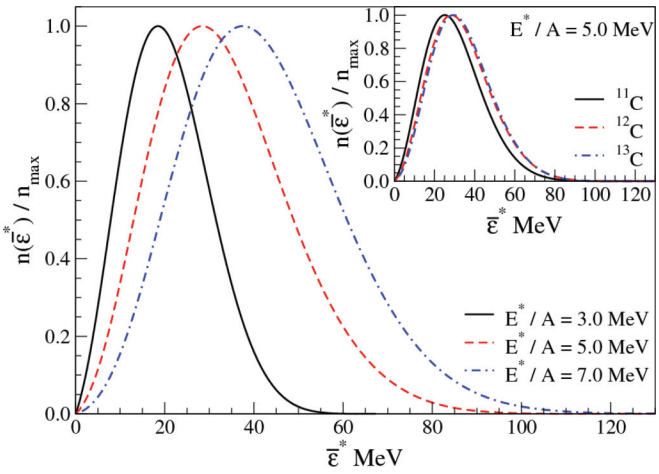

FIG. 3. (Color online) Multiplicity of hot primary ^{12}C as a function of its average excitation energy $\overline{\epsilon}^*$. The fragments are produced in the breakup of ^{40}Ca at different excitation energies, as indicated in the legend. Inset: The same plot for different C isotopes. In this case, the source energy is $E^*/A = 5.0$ MeV. The multiplicities have been scaled by the inverse of the largest value in each case. For details see the text.

also that the width of the distribution is by no means negligible, even at low excitation energies. The inset in Fig. 3 illustrates the isospin dependence of the distribution by displaying $n(\overline{\epsilon}^*)$ for different C isotopes also produced in the breakup of ^{40}Ca at $E^*/A = 5.0$ MeV. It shows that the proton-rich isotope is cooler than the neutron-rich one, which, in its turn, is slightly hotter than ^{12}C. Similar conclusions hold for other species.

Because they are hot, these primary fragments are themselves considered sources and are then allowed to de-excite through the procedure starting at Eq. (18). Given that, in actual experiments, almost all fragments have already decayed by the time they reach the detectors, we apply this procedure successively until the fragment is left in its ground state, if it is stable and does not spontaneously decay by the emission of lighter fragments. In this case, this is treated using the same formalism presented above, with $E^* = 0$.

Thus, once the primary distribution $\{n_{a,z,q}\}$ has been generated, the de-excitation of the fragments follows the steps below.

(i) The average excitation energy $\overline{\epsilon}^*$ of a fragment (A, Z) with energy $q_0\Delta_Q$ is calculated from Eq. (30) and the decay described in Sec. II B is applied to it. The corresponding contribution to the yields of $\{a, z\}$, based on Eq. (22), i.e.,

$$\Delta\overline{n}^{(1)}_{a,z,q} = \overline{n}'_{a,z,q} \times \overline{n}_{A,Z,q_0}, \tag{31}$$

where

$$\overline{n}'_{a,z,q} = \frac{\omega_{a,z,q}}{\Omega_{A,Z,q_0}}\Omega_{A-a,Z-z,q_0-q}, \tag{32}$$

is added to $\overline{n}_{a,z,q}$, $a < A$.

(ii) Because a fragment (A, Z) with energy $q_0\Delta_Q$ will also be produced at this stage, with multiplicity $\overline{n}'_{A,Z,q_0} \times \overline{n}_{A,Z,q_0}$, it will again decay and contribute to the yields of lighter fragments (a, z) in the second step with

$$\Delta\overline{n}^{(2)}_{a,z,q} = \overline{n}'_{a,z,q} \times (\overline{n}'_{A,Z,q_0} \times \overline{n}_{A,Z,q_0}), \tag{33}$$

whereas there will still be a contribution to the yields of (A, Z) equal to $(\overline{n}'_{A,Z,q_0})^2 \times \overline{n}_{A,Z,q_0}$. Thus, the nth step of the decay contributes with

$$\Delta\overline{n}^{(n)}_{a,z,q} = \overline{n}'_{a,z,q} \times ([\overline{n}'_{A,Z,q_0}]^{n-1} \times \overline{n}_{A,Z,q_0}). \tag{34}$$

Because these terms add up at each step, after repeating this procedure until the contribution to (A, Z) tends to 0, i.e., $n \to \infty$, one obtains

$$\overline{n}_{a,z,q} \to \overline{n}_{a,z,q} + \frac{\overline{n}'_{a,z,q}}{1 - \overline{n}'_{A,Z,q_0}} \times \overline{n}_{A,Z,q_0}, \quad a < A. \tag{35}$$

(iii) After carrying out steps i and ii for all the isobars A, one decrements A by one unity and goes back to step (i), until all the excited fragments have decayed.

In order to speed up the calculations, the distribution $n(\overline{\epsilon}^*)$ of the average excitation energies $\overline{\epsilon}^*$ of the decaying fragment (see Fig. 3) is binned in bins of size $\Delta\overline{\epsilon}^*$, for $\overline{\epsilon}^* > 1.0$ MeV. Very low excitation energies, i.e., $0 \leqslant \overline{\epsilon}^* \leqslant 1.0$ MeV, are

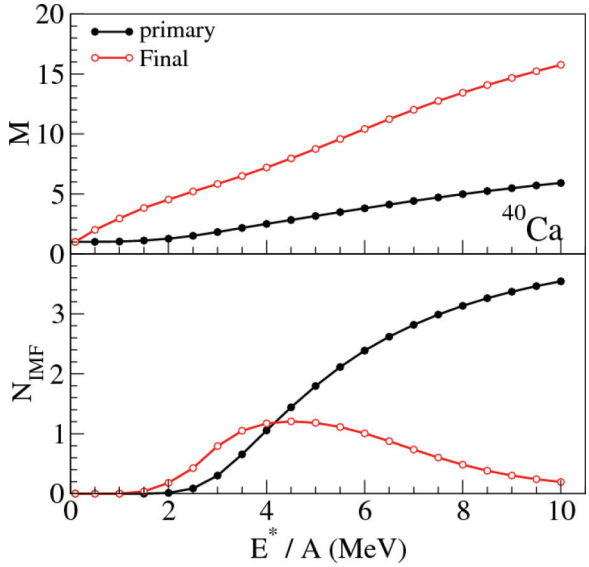

FIG. 4. (Color online) Top: Total fragment multiplicity before and after secondary decay as a function of the total excitation energy of the source. Bottom: IMF multiplicity ($3 \leqslant Z \leqslant 15$) from hot primary fragments and after the de-excitation process. For details see the text.

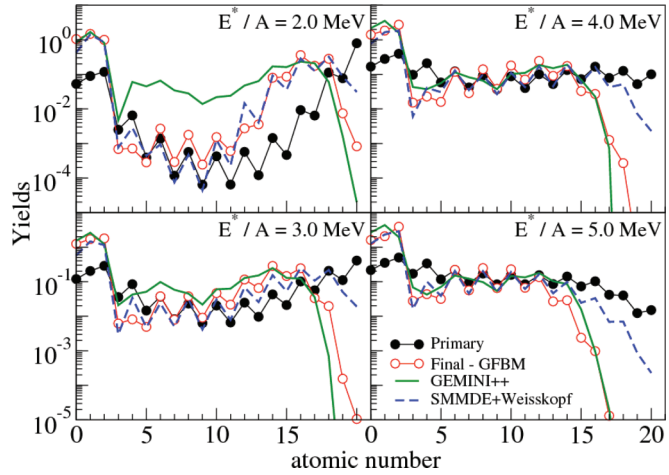

FIG. 5. (Color online) Charge distribution of fragments produced in the breakup of ^{40}Ca at selected excitation energies. The primary distributions are obtained with the SMM-DE, whereas the final yields are calculated with the GFBM presented in this work and also with the Weisskopf-Ewing evaporation model. The predictions of the GEMINI++ code for the decay of a compound nucleus are also displayed. For details see the text.

always grouped in a bin of size 1.0 MeV, regardless of the value of $\Delta\overline{\epsilon}^*$ employed in the calculation.

In Fig. 4 we show the total multiplicity and the number of intermediate-mass fragments (IMFs), $N_{\rm IMF}$, as a function of the total excitation energy E^*/A of the ^{40}Ca source, for both primary and final yields, using $\Delta\overline{\epsilon}^* = 1$ MeV. One sees that the total primary multiplicity M, shown in the upper panel, rises steadily as E^* increases, for $E^*/A \gtrsim 2$ MeV. Up to this point, M is close to unity, which means that the excited source does not decay in the primary stage. On the other hand, when the de-excitation scheme just described is applied to the primary fragments, one also sees in the top panel in Fig. 4 that M increases continuously. It should be noted that most of the fragments are produced in the de-excitation stage. This suggests that the relevance of this stage of the reaction is at least as important as the prompt breakup, for this copious secondary particle emission can hide the underlying physics governing the primary stage.

The lower panel in Fig. 4 displays the multiplicity of IMFs, $N_{\rm IMF}$, as a function of the excitation energy obtained with both the primary and the final yields. It is built by adding up the multiplicities $\overline{n}_{a,z}$ with $3 \leqslant Z \leqslant 15$. The results show that the primary $N_{\rm IMF}$ is 0 for $E^*/A \lesssim 2$ MeV because, up to this point, only the heavy remnant is present, but it quickly departs from 0 at that point, rising steadily from there on. On the other hand, the final $N_{\rm IMF}$ first rises and then falls off because, although fragments with $Z \geqslant 3$ are also produced in the secondary stage, many IMFs are destroyed, as they tend to emit more and more very light fragments ($Z \leqslant 2$) as the excitation energy increases. These results are in qualitative agreement with those presented in Refs. [10] and [11], obtained with different treatments.

The comparison between the primary (filled circles) and the final (open circles) yields obtained with the SMM-DE and the GFBM, respectively, is shown in Fig. 5. One observes that the qualitative shape of the charge distribution does not change appreciably after the de-excitation of the primary hot fragments, but the suppression of heavy residues becomes progressively more important as the excitation energy increases, while the yields of the light fragments are enhanced. These results show that, in the excitation energy domain studied in this work, there are important quantitative differences between the primary and the final charge distributions.

In order to investigate the extent to which our model agrees with others traditionally used in this energy domain, we also display in Fig. 5 the results obtained with the GEMINI++ code (solid lines) [3–5]. We considered the reaction ^{20}Ne + ^{20}Ne, at the appropriate bombarding energy, leading to a compound nucleus equal to ^{40}Ca with the suitable excitation energy. One observes a very good agreement with the predictions made by the GEMINI++ code and the GFBM, which systematically improves as the excitation energy of the source increases. This is probably caused by the different assumptions made by the two models, i.e., binary emission versus prompt breakup, which seem to affect the charge distribution only at very low excitation energies. To further investigate these aspects, it is useful to consider another traditional treatment. In this way, we also show, in Fig. 5, the final yields obtained by applying the Weisskopf-Ewing evaporation model, described in Refs. [25] and [26], to the de-excitation of the primary SMM-DE fragments. The corresponding results are represented by dashed lines. The agreement with the GFBM is very good, except for the heavier fragments, as the Weisskopf-Ewing model gives much larger contributions in this charge/mass region than the GFBM.

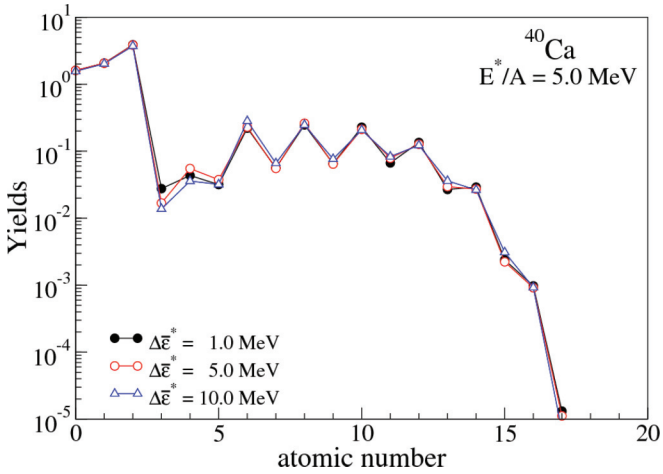

FIG. 6. (Color online) Charge distribution of fragments produced in the breakup of ^{40}Ca at $E^*/A = 5.0$ MeV. All the parameters of the calculation are kept fixed, except for $\Delta\bar{\epsilon}^*$. For details see the text.

Similar conclusions hold for the comparison with the GEMINI model. In the Weisskopf-Ewing treatment, very light particles tend to carry a large fraction of the excitation energy, leaving a heavy remnant weakly excited. This leads to the overprediction of yields of heavy fragments, compared with the GFBM and the GEMINI model. Detailed comparisons with experimental data will help to select the best scenario for the de-excitation process.

Finally, we examine the sensitivity of the model results to the binning used to speed up the calculations in the secondary decay stage. The charge distributions for the breakup of ^{40}Ca at $E^*/A = 5.0$ MeV is displayed in Fig. 6 for $\Delta\bar{\epsilon}^* = 1.0$, 5.0, and 10.0 MeV. It is clear that the charge distribution is weakly affected by this parameter so that values within this range may be safely used, as the variations are within the model's precision.

IV. CONCLUDING REMARKS

We have presented an implementation of the GFBM, introduced in Ref. [14], to treat the de-excitation of the primary hot fragments produced in the breakup of a nuclear source. The approach is based on the SMM [15–17,24], which describes the primary breakup stage. It is then successively applied to the primary fragments until they have decayed to the ground state. Because the application of the SMM to all the primary fragments, repeatedly until they are no longer excited, would be extremely time-consuming, we have developed an implementation of the SMM based on the recursion formulas presented in Ref. [21]. Those formulas allow the statistical weights to be very efficiently computed so that they make the application of our model to systems of interest feasible. We found that the traditional Monte Carlo implementation of the SMM and that developed in the present work lead to very similar results, so that either one may be used according to the need. Furthermore, the similarity of the final yields obtained with our GFBM with those predicted by the GEMINI++ code strongly suggests that our treatment is at least as good as the more traditional ones. Compared to the Weisskopf-Ewing evaporation model, a very good agreement is obtained at all the excitation energies studied. Important deviations are observed only in the large mass/charge region, as the Weisskopf-Ewing model overpredicts the corresponding yields. Applications to other systems and comparisons with experimental data are in progress, which should contribute to improving the de-excitation treatments.

ACKNOWLEDGMENT

We would like to acknowledge the CNPq, a FAPERJ BBP grant, the FAPESP, and the joint PRONEX initiatives of CNPq/FAPERJ under Contract No. 26-111.443/2010 for partial financial support. This work was supported in part by the National Science Foundation under Grants No. PHY-0606007 and No. INT-0228058.

[1] N. Bohr and J. A. Wheeler, Phys. Rev. **56**, 426 (1939).
[2] V. F. Weisskopf and D. H. Ewing, Phys. Rev. **57**, 472 (1940).
[3] R. J. Charity, M. A. McMahan, G. J. Wozniak, R. J. McDonald, L. G. Moretto, D. G. Sarantites, L. G. Sobotka, G. Guarino, A. Pantaleo, L. Fiore, A. Gobbi, and K. D. Hildenbrand, Nucl. Phys. A **483**, 371 (1988).
[4] R. J. Charity, Phys. Rev. C **82**, 014610 (2010).
[5] D. Mancusi, R. J. Charity, and J. Cugnon, Phys. Rev. C **82**, 044610 (2010).
[6] A. J. Cole, *Statistical Models for Nuclear Decay: From Evaporation to Vaporization* (IOP, Philadelphia, 2000).
[7] E. Fermi, Prog. Theor. Phys. **5**, 570 (1950).
[8] E. Fermi, Phys. Rev. **81**, 683 (1951).
[9] A. S. Botvina, A. S. Iljinov, I. N. Mishustin, J. P. Bondorf, R. Donangelo, and K. Sneppen, Nucl. Phys. A **475**, 663 (1987).
[10] J. P. Bondorf, A. S. Botvina, A. S. Iljinov, I. N. Mihustin, and K. Sneppen, Phys. Rep. **257**, 133 (1995).
[11] W. P. Tan, S. R. Souza, R. J. Charity, R. Donangelo, W. G. Lynch, and M. B. Tsang, Phys. Rev. C **68**, 034609 (2003).
[12] C. B. Das, S. Das Gupta, W. G. Lynch, A. Z. Mekjian, and M. B. Tsang, Phys. Rep. **406**, 1 (2005).
[13] W. Hauser and H. Feshbach, Phys. Rev. **87**, 366 (1952).
[14] B. V. Carlson, R. Donangelo, S. R. Souza, W. G. Lynch, A. W. Steiner, and M. B. Tsang, Nucl. Phys. A **876**, 77 (2012).
[15] J. P. Bondorf, R. Donangelo, I. N. Mishustin, C. J. Pethick, H. Schulz, and K. Sneppen, Nucl. Phys. A **443**, 321 (1985).
[16] J. Bondorf, R. Donangelo, I. N. Mishustin, and H. Schulz, Nucl. Phys. A **444**, 460 (1985).
[17] K. Sneppen, Nucl. Phys. A **470**, 213 (1987).
[18] K. C. Chase and A. Z. Mekjian, Phys. Rev. C **52**, R2339 (1995).
[19] S. Das Gupta and A. Z. Mekjian, Phys. Rev. C **57**, 1361 (1998).
[20] P. Bhattacharyya, S. Das Gupta, and A. Z. Mekjian, Phys. Rev. C **60**, 054616 (1999).
[21] S. Pratt and S. Das Gupta, Phys. Rev. C **62**, 044603 (2000).
[22] S. R. Souza, W. P. Tan, R. Donangelo, C. K. Gelbke, W. G. Lynch, and M. B. Tsang, Phys. Rev. C **62**, 064607 (2000).

[23] E. Wigner and F. Seitz, Phys. Rev. **46**, 509 (1934).
[24] S. R. Souza, P. Danielewicz, S. Das Gupta, R. Donangelo, W. A. Friedman, W. G. Lynch, W. P. Tan, and M. B. Tsang, Phys. Rev. C **67**, 051602(R) (2003).
[25] S. R. Souza, M. B. Tsang, B. V. Carlson, R. Donangelo, W. G. Lynch, and A. W. Steiner, Phys. Rev. C **80**, 041602(R) (2009).
[26] S. R. Souza, R. Donangelo, W. G. Lynch, and M. B. Tsang, Phys. Rev. C **76**, 024614 (2007).